Int. J. Solids Structures Vol. 29, No. 19, pp. 2355–2367, 1992
Printed in Great Britain.

0020–7683/92 $5.00 + .00

ELASTIC WAVE SCATTERING BY CRACKS AND INCLUSIONS IN PLATES: IN-PLANE CASE

M. R. KARIM
The Ralph M. Parsons Company, 100 West Walnut Street, Pasadena, CA 91124, U.S.A.

and

M. A. AWAL and T. KUNDU
Department of Civil Engineering and Engineering Mechanics, University of Arizona, Tucson, AZ 85721, U.S.A.

(*Received* 10 *June* 1991; *in revised form* 25 *January* 1992)

Abstract—The scattering of elastic waves in a plate by a distribution of inclusions and/or cracks within a finite zone is studied by a combination of analytical and finite element methods. The incident field is generated by either a time harmonic beam of finite width or guided waves. A part of the plate containing the inclusions/cracks (interior region) is modeled by conventional finite elements. The far-field (exterior region) is approximated by a number of guided (Lamb) wave modes with real wave numbers. The scattered and total fields (displacements and stresses) are obtained by matching the two regions to satisfy the displacement and stress compatibilities at the near field–far field boundary. Numerical results are presented showing the effects of cracks and inclusions in a plate.

1. INTRODUCTION

Plates containing inclusions such as rivets and welds are often used in industry. Cracks in plates, especially those with inclusions, are also common place. Whenever inclusions and/or cracks are present in any structure two important questions often asked are: (1) can the very small cracks/inclusions be detected? and (2) what is the effect of cracks/inclusions on the stiffness of the plate? Ultrasonic non-destructive evaluation (NDE) is a very useful technique for detecting subsurface cracks/inclusions and measuring the resulting stiffness changes (Duke *et al.*, 1986). But except for highly idealized cases it is very difficult and sometimes impossible to obtain analytical solutions to the problems with inclusions and cracks. The problem is also very difficult to solve by finite element methods as inclusions/cracks are usually present in a very small region of a plate with very large lateral dimensions. The best way to solve the problem will be to take advantages of both the finite element and analytical methods. In this study an approach is pursued with the ultimate objective of detecting cracks/inclusions in a plate and to assess the effects of inclusions/cracks on the plate stiffness. The solution to the corresponding anti-plane problem was presented by Karim *et al.* (1992); references to previous studies for related problems can be found in Paskaramoorthy *et al.* (1989) and also in Karim *et al.* (1992).

In recent years considerable progress has been made in understanding the ultrasonic NDE experiments. Most of the ultrasonic NDE studies, however, were limited to acoustic microscopy (Kundu, 1988) and leaky Lamb wave (Karim *et al.*, 1990) experiments, where test specimens are submerged in a fluid. For most real life structures such as airplanes and automobiles, it is unrealistic to submerge the whole structure under a fluid for NDE purposes. A more realistic idea is to attach a source transducer at some point on the surface of the structure and to detect the resulting surface response by a receiving transducer placed at some other point. Traditionally, noise generated by such a setup was too great to be separated from the signal. Recently, Duke *et al.* (1986) have perfected such an experimental setup whereby noise to signal ratio is reduced to a low value. In this study, we will present a near field finite element analysis combined with the far field analytical solution to simulate the surface source/surface receiver ultrasonic NDE experiments. We will restrict ourselves to solving the direct problem, i.e. calculating the surface response due to applied surface

source on a plate with a known distribution of cracks and or inclusions. Once the solution of the direct problem is obtained, solution of the inverse problem, namely detecting cracks (not necessarily parallel to the plate surface), and estimating resulting stiffness reduction is straightforward (Tang and Henneke, 1989; Karim *et al.*, 1990).

In the past most of the studies involving interior and exterior regions for wave scattering by cracks and inclusions were devoted to either half-space or full space (Avanessian *et al.*, 1989). Only Paskaramoorthy *et al.* (1989) studied the flexural wave scattering by a through crack in a plate. In most of these studies eigenfunction expansions for the wave equations were used to simulate the far-field behavior. Karim *et al.* (1992) were the first to propose the idea of using guided waves with real roots to simulate the far-field behavior in such an analysis. Using guided waves has a distinct advantage over using wave function expansion in plate problems; they automatically satisfy the stress-free boundary conditions thereby avoiding the complicated zero-energy integrals prescribed to satisfy the traction-free boundary conditions in global–local finite element analysis (Avanessian *et al.*, 1989).

In the numerical model, a finite region containing all the inclusions and cracks is modeled by eight node isoparametric finite elements. The singularity characteristics of the crack tip are modeled by quarter point elements (Henshell and Shaw, 1975; Barsoum, 1976) and one row of transition elements (Lynn and Ingraffea, 1978). In the exterior region, the radiated fields are modeled by Lamb waves, which satisfy the stress-free boundary conditions at the plate surfaces. Only Lamb waves with the real wave numbers are considered. The contributions due to guided waves with complex wave numbers are neglected as their effects on the overall solution are very small if the finite element zone is sufficiently large. Only time harmonic problems are considered in the present study. The time histories can be easily obtained from the time harmonic results by means of highly efficient fast Fourier transform (FFT) algorithm.

2. FORMULATION OF THE PROBLEM

We consider time harmonic excitations acting on an infinite plate of finite thickness, $2h$, and elastic constants, λ, μ and density, ρ. We assume that the plate occupies the region $-\infty < (x, y) < \infty$, $-h < z < h$ relative to a Cartesian co-ordinate system located within the plate (Fig. 1) and contains a number of inclusions and/or cracks. We further assume that the external loads are either a finite beam of width $2b$ on the plate surface within the finite element zone or a source located at $x = -\infty$ and both surfaces of the plate are traction free in the exterior regions. In addition crack surfaces are assumed to remain stress free over the entire load cycle. To achieve this in reality the cracks would have to be initially opened by some static preload or some other means and the dynamic solution would be superimposed on this initial state. The source and all the field quantities are independent of y and have a time dependence $e^{-i\omega t}$, which is suppressed in all the subsequent representations. When necessary, superscripts i and r will be used to indicate variables associated with the incident and radiated wave fields and subscripts I and B will be used to distinguish between the interior and boundary variables.

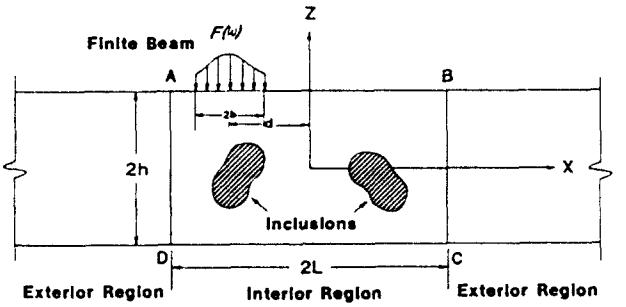

Fig. 1. A Schematic diagram of the problem geometry.

2.1. *Finite element model*

The motion of the region, $-L < x < L$, containing all the cracks/inclusions may be perceived as forced vibration. Following the conventional discretization process in the finite element methodology element equation satisfying the governing equations can be written as

$$[K]\{V\} = \{Q\}, \tag{1}$$

where $[K]$ is the generalized stiffness matrix that also includes the inertia effect, $\{V\}$ is the vector of nodal displacements and $\{Q\}$ is the consistent load vector. The stiffness matrix for the in-plane harmonic propagation can be written as

$$[K] = \iint_A [B]^T[C][B]\,dA - \rho\omega^2 \iint_A [N]^T[N]\,dA, \tag{2}$$

where $[N]$ is the matrix of interpolation functions, $[B]$ is the strain displacement transformation matrix, $[C]$ is the plane strain constitutive matrix and ω is the circular frequency. In (2), the first and second integrals are typical stiffness and mass matrices used in conventional finite element codes.

If the vector of nodal variables is separated into two parts: $\{V_B\}$ corresponding to the nodal variables at the boundaries AD and BC (Fig. 1) and $\{V_I\}$ corresponding to nodal variables elsewhere, (1) can be written as

$$\begin{bmatrix} K_{II} & K_{IB} \\ K_{BI} & K_{BB} \end{bmatrix} \begin{Bmatrix} V_I \\ V_B \end{Bmatrix} = \begin{Bmatrix} Q_I \\ Q_B \end{Bmatrix}, \tag{3}$$

where $\{Q_I\}$ and $\{Q_B\}$ are the nodal forces corresponding to V_I and V_B, respectively. If $\{Q_I\}$ and $\{Q_B\}$ are known, the displacements can be obtained by solving (3).

It should be noted that the matrix $[K]$ becomes singular when the incident wave frequency, ω, coincides with the natural frequency of the interior region and care must be taken to avoid these frequencies in the numerical implementation of the present technique.

2.2. *Guided wave mode expansions*

In the exterior region, the displacement field, V, consists of the incident wave field V^i and the radiated wave field V^r as follows,

$$V = V^i + V^r, \quad x < -L, \qquad V = V^r, \quad x > L. \tag{4a, b}$$

The radiated displacement fields satisfying the governing equations and the traction-free boundary conditions can be expressed as symmetric and anti-symmetric Lamb waves (Mal and Singh, 1990). In the subsequent representations superscripts S and A will be used to distinguish between the symmetric and anti-symmetric fields.

The radiated displacement fields due to symmetric Lamb waves propagating in the positive x-direction can be written as

$$U^{Sr} = \sum_{m=1}^{n} S_m \left[\frac{(2k_m^2 - k_2^2)^2 \sinh(\eta_{m2}h)}{2\eta_{m1} \sinh(\eta_{m1}h)} \cosh(\eta_{m1}z) - \eta_{m2} \cosh(\eta_{m2}z) \right] e^{ik_m x}$$

$$= \sum_{m=1}^{p} S_m U_m^{Sr}$$

$$W^{Sr} = \sum_{m=1}^{p} S_m \left[\frac{(2k_m^2 - k_2^2)^2 \sinh(\eta_{m2}h)}{2ik_m \sinh(\eta_{m1}h)} \sinh(\eta_{m1}z) - ik_m \sinh(\eta_{m2}z) \right] e^{ik_m x}$$

$$= \sum_{m=1}^{p} S_m W_m^{Sr} \tag{5}$$

and k_m is the real root of the symmetric dispersion equation

$$\frac{\tanh(\eta_{m2}h)}{\tanh(\eta_{m1}h)} = \frac{4k_m^2\eta_{m1}\eta_{m2}}{(2k_m^2-k_2^2)^2}, \tag{6}$$

where

$$\eta_{mj} = (k_m^2 - k_j^2)^{\frac{1}{2}}, \quad j = 1, 2.$$

Symmetric Lamb waves propagating in the negative x-direction are given by the complex conjugate of (5). k_1 and k_2 are the longitudinal and shear wave numbers respectively and S_m is the as yet unknown amplitude of the mth symmetric mode. U and W are the displacements in the x and z-directions respectively.

Similarly, the radiated displacement fields for the anti-symmetric Lamb waves propagating in the positive x-direction are given by

$$\begin{aligned} U^{Ar} &= \sum_{n=1}^{q} A_n \left[ik_n \sinh(\eta_{n1}z) + \frac{(2k_n^2-k_2^2)^2 \sinh(\eta_{n1}h)}{2ik_n \sinh(\eta_{n2}h)} \sinh(\eta_{n2}z) \right] e^{ik_n x} \\ &= \sum_{n=1}^{q} A_n U_n^{Ar} \\ W^{Ar} &= \sum_{n=1}^{q} A_n \left[\eta_{n1} \cosh(\eta_{n1}z) - \frac{(2k_n^2-k_2^2)^2 \sinh(\eta_{n1}h)}{2\eta_{n2} \sinh(\eta_{n2}h)} \cosh(\eta_{n2}z) \right] e^{ik_n x} \\ &= \sum_{n=1}^{q} A_n W_n^{Ar} \end{aligned} \tag{7}$$

and k_n is the real root of the anti-symmetric dispersion equation

$$\frac{\tanh(\eta_{n2}h)}{\tanh(\eta_{n1}h)} = \frac{(2k_n^2-k_2^2)^2}{4k_n^2\eta_{n1}\eta_{n2}}, \tag{8}$$

where

$$\eta_{nj} = (k_n^2 - k_j^2)^{1/2}, \quad j = 1, 2.$$

A_n is the as yet unknown amplitude of nth anti-symmetric mode.

The total radiated field is simply the sum of the symmetric and anti-symmetric fields

$$U^r = U^{Sr} + U^{Ar} \quad W^r = W^{Sr} + W^{Ar}. \tag{9}$$

Once the radiated displacement fields are known, corresponding stress fields can easily be obtained by using stress–displacement relations.

The incident field, V^i, can be any of the n guided wave modes or zero (when the load is applied within the finite element zone). The solutions due to a number of incident guided wave modes can be obtained by adding the solutions of individual guided wave modes.

2.3. *Global solution*

After obtaining the wave fields in the interior and exterior regions, the nodal displacements are obtained by imposing the following continuity conditions of the displacements and tractions at the boundary nodes

$$\{V_B\} = \{V_B^i\} + \{V_B^r\}; \quad \text{on AD} \qquad = \{V_B^r\}; \quad \text{on BC} \tag{10a, b}$$

$$\{Q_B\} = \{Q_B^i\} + \{Q_B^r\}; \quad \text{on AD} \qquad = \{Q_B^r\}; \quad \text{on BC.} \tag{11a, b}$$

Recall that the incident field is given and the radiated field is to be represented by a complete set of known wave mode expansions (5) and (7), whose amplitudes remain undetermined.

Suppose that the incident field is expressed by the first $p+q$ wave mode expansions as

$$V^i = \sum_{M=1}^{p+q} a_M \{V_M\}, \tag{12}$$

where, for $M = 1$ to p

$$\{V_M\} = \begin{Bmatrix} U_M^{Sr} \\ W_M^{Sr} \end{Bmatrix}, \tag{13a}$$

and for $M = p+1$ to $p+q$

$$\{V_M\} = \begin{Bmatrix} U_{M-p}^{Ar} \\ W_{M-p}^{Ar} \end{Bmatrix} \tag{13b}$$

and a_M is the amplitude of the Mth guided wave mode. Then the nodal displacements at the mesh boundaries for the incident wave have the form

$$V_B^i = \sum_{M=1}^{p+q} a_M \{V_{BM}\}, \tag{14}$$

where $\{V_{BM}\}$ denotes the column vector obtained from $\{V_M\}$ evaluated at the boundary nodes.

From the incident displacement field, one can calculate the stresses that would occur on the finite element boundaries. The tractions due to these stresses may be regarded as known forcing functions on the finite element mesh. The nodal forces associated with these tractions can be calculated following the conventional finite element technique, i.e. by integrating the product of the tractions with the finite element displacement interpolations over the mesh boundary. Let us denote the nodal forces on the mesh boundary associated with $\{V_{BM}\}$ by $\{Q_{BM}\}$. The load vector for the incident wave, the right-hand side of eqn (3), can be written as

$$Q_B^i = \sum_{M=1}^{p+q} a_M \{Q_{BM}\}. \tag{15}$$

Suppose that the radiated waves in question can be expressed with sufficient accuracy with P symmetric and Q anti-symmetric modes in the form

$$V^r = \sum_{N=1}^{P+Q} b_N \{V_N\}, \tag{16}$$

where b_N are the unknown amplitudes to be determined. Analogously as for the incident waves, the degrees of freedom at the boundary and the consistent load vectors associated with the scattered displacements of eqn (13) have the form,

$$V_B^r = \sum_{N=1}^{P+Q} b_N \{V_{BN}\} \qquad Q_B^r = \sum_{N=1}^{P+Q} b_N \{Q_{BN}\}, \tag{17, 18}$$

where $\{Q_{BN}\}$ is the nodal force associated with $\{V_{BN}\}$ in (17).

To enforce the stress and displacement continuity, we combine the boundary stresses and displacements due to the incident and radiated waves as

$$\{V_B\} = \{V_B^i\} + \{V_B^r\} = \sum_{M=1}^{p+q} a_M \{V_{BM}\} + \sum_{N=1}^{P+Q} b_N \{V_{BN}\} \tag{19a}$$

$$\{Q_B\} = \{Q_B^I\} + \{Q_B^S\} = \sum_{M=1}^{P+q} a_M\{Q_{BM}\} + \sum_{N=1}^{P+Q} b_N\{Q_{BN}\}. \tag{19b}$$

Combining (3) and (19), after some simplifications we can write

$$[A]\{b\} = \{P\}, \tag{20}$$

where

$$[A] = [[K_{BB}] - [K_{BI}][K_{II}]^{-1}[K_{IB}]]\{V_{BN}\} - \{Q_{BN}\} \tag{21a}$$

$$[P] = \sum_{M=1}^{P+q} a_M(\{Q_{BM}\} - [[K_{BB}] - [K_{BI}][K_{II}]^{-1}[K_{IB}]]\{V_{BM}\}) \tag{21b}$$

and b is a $(P+Q) \times 1$ array of the still unknown coefficients b_n.

In (21), the applied load is assumed to be due to a guided wave source located at $x = -\infty$, i.e. $\{Q_I\}$ in (3) is assumed to be a null matrix. If the source is located within the finite element zone, (21) should be adjusted properly.

Let m be the number of degrees of freedom on the boundary AD and BC, then $[A]$ has the dimensions $m \times (P+Q)$. Three cases of the relative dimensionality of the algebraic system, (20) can be distinguished:

(1) $m > P+Q$—overdeterminate.
(2) $m = P+Q$—consistent.
(3) $m < P+Q$—underdeterminate.

The solution to (20) may be expressed as a least squares error minimization. Let us define an error function $\{\varepsilon\}$ by

$$\{\varepsilon\} = [A]\{b\} - \{P\}. \tag{22}$$

The square of the error ε^2 is constructed by multiplying (22) by its conjugate transpose $\{\varepsilon^*\}^T$, i.e.

$$\begin{aligned}\{\varepsilon\}^2 &= \{\varepsilon^*\}^T\{\varepsilon\} \\ &= \{b^*\}^T[A^*]^T[A]\{b\} - \{P^*\}^T[A]\{b\} - \{b^*\}^T[A^*]^T\{P\} + \{P^*\}^T\{P\}.\end{aligned} \tag{23}$$

Minimizing the square of the error, ε^2, with respect to undetermined coefficients b_N yields

$$[A^*]^T[A]\{b\} = [A^*]^T\{P\}. \tag{24}$$

Thus, the coefficient vector $\{b\}$ of the radiated field is given by

$$\{b\} = ([A^*]^T[A])^{-1}[A^*]^T\{P\}. \tag{25}$$

For $m \geq P+Q$ the matrix operation $([A^*]^T[A])^{-1}[A^*]^T$ is the generalized inverse of $[A]$ and the uniqueness of the solution to (20) as given by (25) is assured (Lancaster, 1969). The case $m < P+Q$ does not seem to occur in a reasonably planned numerical work and will not be pursued here. Once the coefficients b_n are determined, the displacements and stresses at any interior or exterior point can easily be obtained.

3. NUMERICAL RESULTS

The method discussed above has been implemented in a FORTRAN program. To verify the program, normal surface displacement of a 2 mm thick aluminum plate due to a

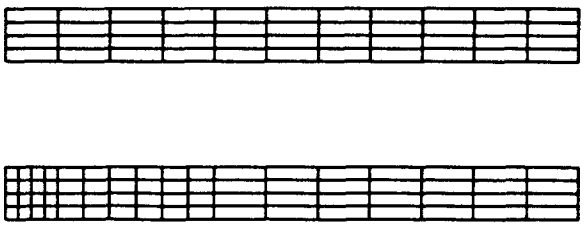

Fig. 2. One quarter of the finite element mesh of the interior region. The top figure is for 176 elements and the bottom figure is for 272 elements.

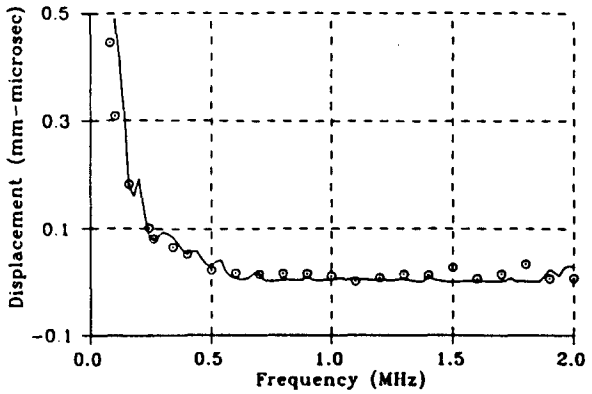

Fig. 3. Normal (vertical) surface displacement of a 1 mm thick aluminum plate due to normal (vertical) surface line load at a distance of 10 mm. Solid line is for present numerical model, odots (⊙) are analytical results (Xu and Mal, 1987).

normal surface line source at a distance of 10 mm is computed by this method and compared with the analytical Green's function solution (Xu and Mal, 1987) in Fig. 3. The homogeneous plate is first subdivided into two regions, an interior region and an exterior region. The interior region is discretized into 176 uniform eight noded isoparametric elements. One quarter of the discretized interior region is shown in the top of Fig. 2. Guided wave modes are considered in the exterior region. Computed results from this analysis are shown by the continuous line in Fig. 3. Results obtained by the Green's function approach described in Xu and Mal (1987) are given by odots in Fig. 3. Further refining of the mesh to 272 eight-noded isoparametric elements (quarter of the plate is shown in the bottom of Fig. 2) didn't change the final results, so such refinement is not necessary for the uniform plate analysis. The material properties used by Xu and Mal (1987) are shown in Table 1.

q_1 and q_2 are the quality factors which account for the viscoelastic properties of the solid. In the present analysis, quality factors are assumed to be ∞; in other words, the material is assumed to be purely elastic. Agreement between the numerical and analytical results can be seen to be excellent; very small discrepancies can be attributed to the different values of the viscoelastic parameters in the two analyses.

For all the subsequent analyses, the incident field is assumed to have the following form:

$$P = f(t)F(x), \tag{26}$$

Table 1. Material properties

Materials	Density gm cc^{-1}	P-wave velocity mm μs^{-1}	SV-wave velocity mm μs^{-1}	Quality factors q_1	q_2
Aluminum	1.50	4.00	2.00	520	300
Rivet/weld	2.77	6.37	3.16		

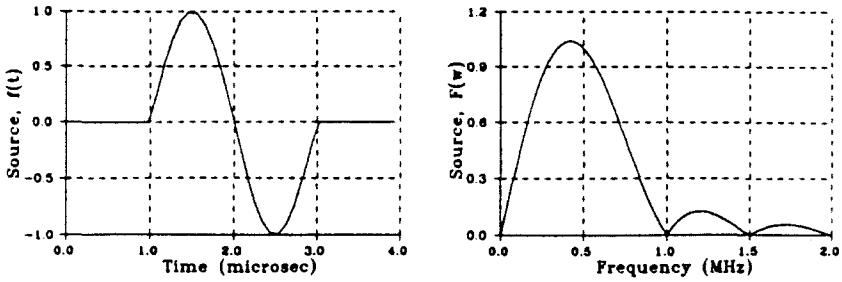

Fig. 4. Variation of source function with time and its Fourier transform.

$$f(t) = \begin{cases} 0 & t \leqslant T \\ A \sin\{2\pi(t-T)/\tau\} & T \leqslant t \leqslant T+\tau, \\ 0 & t \geqslant T+\tau \end{cases} \tag{27a}$$

$$F(x) = \begin{cases} \exp[-\{(x+d)/b\}^2], & |x| \leqslant b \\ 0, & |x| \geqslant b \end{cases}, \tag{27b}$$

where $f(t)$ and $F(x)$ are the temporal and spatial distributions of applied load. In (27a), "A" defines the peak value of the load, τ is the duration of the load and T is the time of load application. In (27b), b is the half-width of the applied load and d is the offset of the center of the load from the origin as shown in Fig. 1. The sharpness of the load can be increased by decreasing τ but keeping A constant. In the results presented here, the peak value of the load, A, is taken as 1 kN mm^{-1}, the duration of the load, τ, is taken as 2 μs and the time of loading T is taken as 1 μs. The variation of the loading function with time, $f(t)$, and its Fourier transform, $F(\omega)$ are shown in Fig. 4.

In Fig. 5 the bottom figure shows the problem geometry and the top figure shows the quarter of the finite element mesh of the interior region. The mesh has 240 eight-noded isoparametric elements. Element size is selected such that the elements are not too big compared to the wave length of the induced elastic waves in the plate. For a detailed

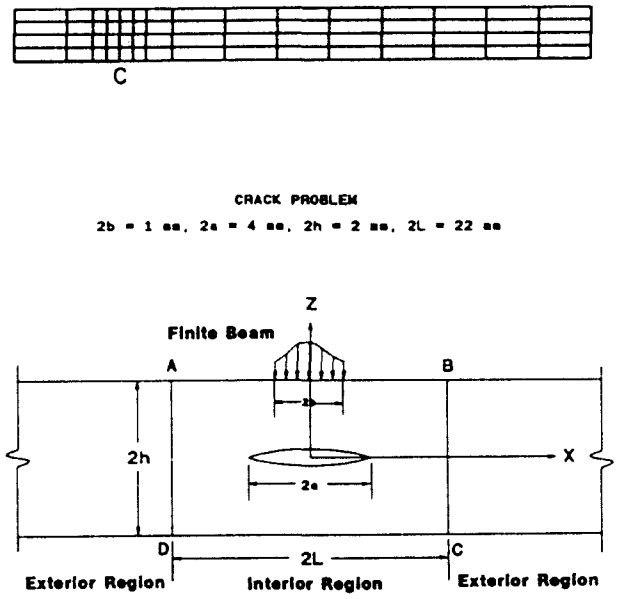

Fig. 5. Schematic diagram of a cracked plate geometry (bottom figure) and one quarter of the finite element mesh of the interior region (top figure). The crack tip is denoted by point C in the top figure.

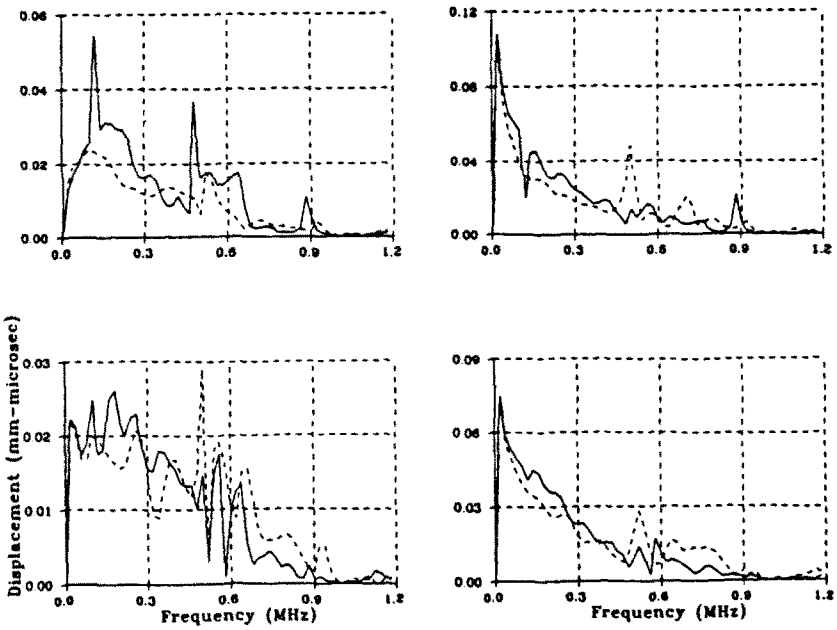

Fig. 6. Surface displacement of a cracked plate due to a vertical surface load with a Gaussian spatial variation as shown in Fig. 4. and eqn (27b). Top and bottom rows are displacements at points (2.0, 1.0) and (10.0, 1.0) respectively. Left column shows the horizontal displacement and right column shows the vertical displacement. Solid line shows the displacement due to a cracked plate and dashed line is for the uncracked plate.

discussion of the element size requirement, readers are referred to Kundu and Hassan (1987) and Romanel and Kundu (1990). The crack tip is denoted by point C in the mesh. Elements are refined near the crack tip as shown. Elements adjacent to the crack tip are changed to quarter point elements to handle the stress singularity (Henshel and Shaw, 1975; Barsoum, 1976). One layer of transition elements (Lynn and Ingraffia, 1978) is also placed between quarter point elements and conventional eight noded elements to obtain more accurate results. Thus the requirement of a very fine mesh near the crack tip is avoided. Dimensions of various quantities are given in Fig. 5. No significant change in the result is obtained when the length of the interior region is increased. Figure 6 shows the surface response of the cracked plate shown in Fig. 5.

Solid and dotted lines in Fig. 6 correspond to the surface displacements of cracked and uncracked plates respectively. Left and right columns show two components of the displacement and two rows correspond to two points on the surface, as mentioned in the figure caption. From Fig. 6 it is evident that the number and positions of the minima of the displacement spectra, which are of primary interest in the NDE experiments, change significantly by the presence of the crack. Changes in the magnitude of the displacement spectra, however, are small. The effect of the crack can be felt strongly even at a relatively large distance (five times the plate thickness) from the crack. This is due to the fact that the material properties of the plate are assumed to be purely elastic and there is no geometric damping for the guided waves.

Effect of the crack orientation and the interaction effect between the cracks are then studied and shown in Fig. 9 for the crack geometries shown in Fig. 7. One quarter of the finite elements mesh of the interior region for every problem geometry of Fig. 7 is shown in Fig. 8. For the single crack problem (both horizontal and vertical cracks) the region is discretized into 256 elements. For the double crack geometry this number is increased to 264 elements. Discretization of the right side of the plate is kept unchanged (similar to the middle figure) but in the left side, elements are refined near the second crack as shown at the bottom of Fig. 8. Crack tip positions are indicated by point C in every mesh. Here also, quarter point elements and transition elements are used as mentioned in the previous case.

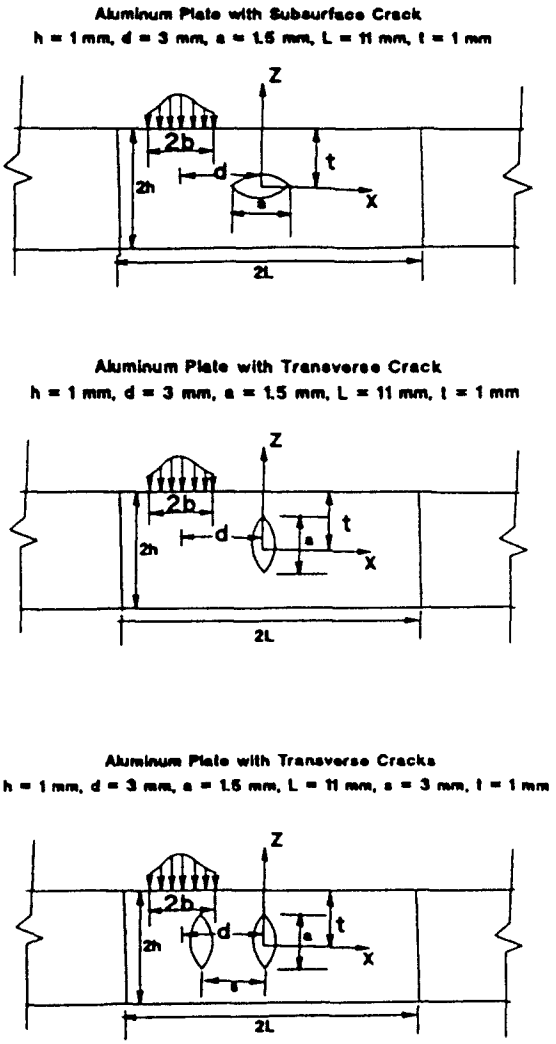

Fig. 7. Schematic diagram of different cracked plates whose responses are given in Fig. 9.

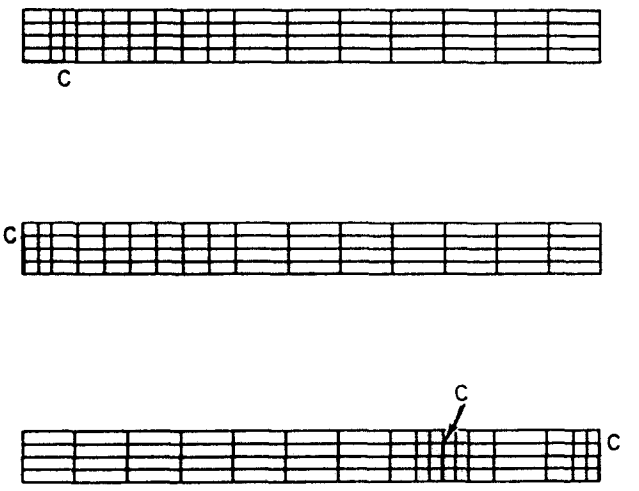

Fig. 8. One quarter of the finite element mesh of the interior regions of the three problem geometries shown in Fig. 7. C indicates the crack tip position.

Convergence of the solution was studied by changing the coordinate values of different nodes. No significant change was noted.

Cracks in an object reduces its stiffness. So surface displacements are affected by the presence of internal cracks. Karim and Kundu (1990) found that for a half-space the displacement spectra become larger in the presence of a crack. However, for the plate problem considered here, the displacements of the cracked plate are sometimes found to be smaller than that of an uncracked plate.

The effect of a rivet, as shown in Fig. 10, on the surface response of a plate, is shown in Fig. 11. The finite element mesh shown at the foot of Fig. 2 is used here, properly changing the material properties of the elements which occupy the rivet position. Properties of the rivet materials, which usually have a higher stiffness than the plate itself, are shown in Table 1. The magnitude of the displacement spectra is changed significantly. This is due to the large scattering surface and a number of sharp corners in the rivet.

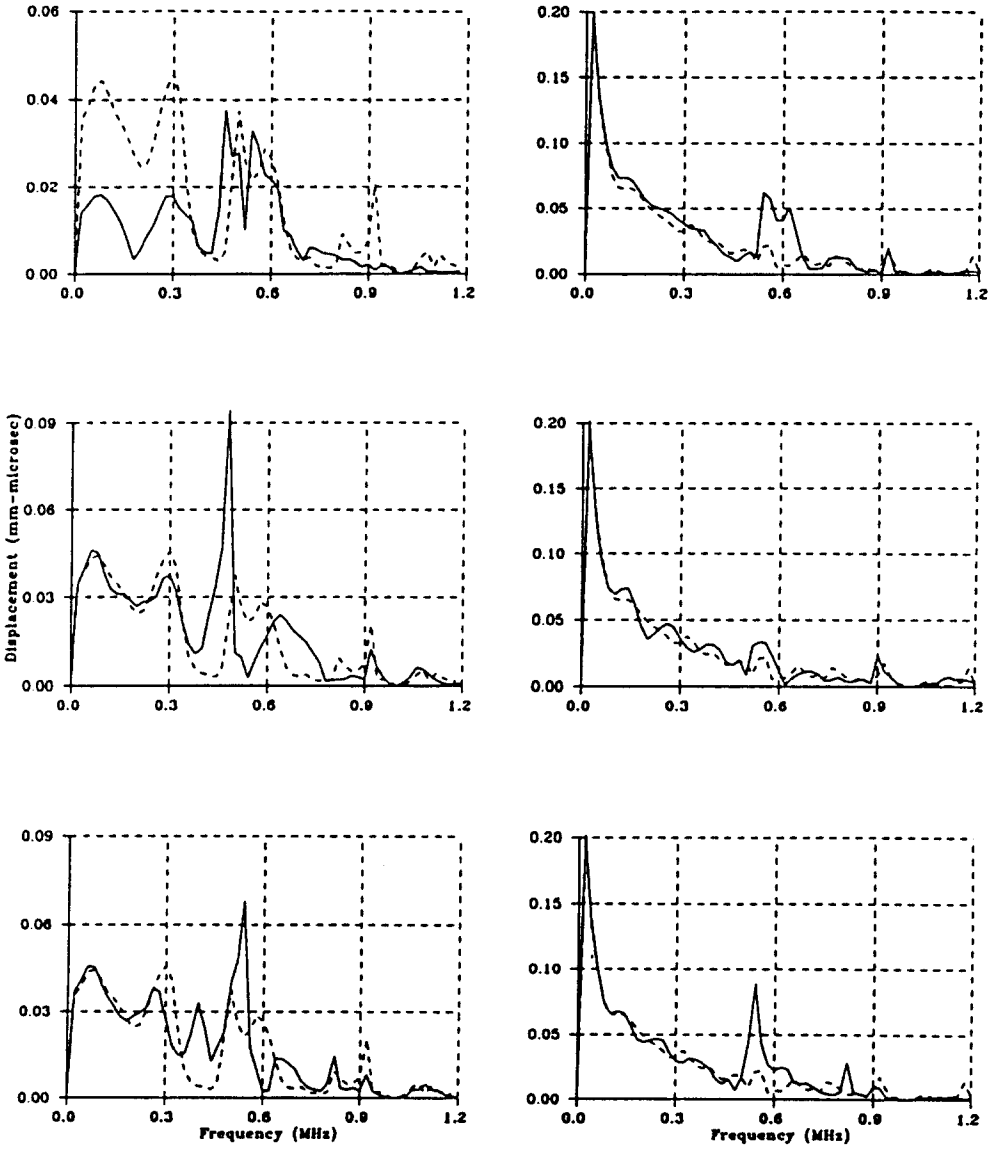

Fig. 9. Top, middle and bottom rows show the surface displacement at point (2.0, 1.0) in three plate geometries shown in Fig. 7. Left and right columns show the horizontal and vertical displacements respectively. Dashed line in each plot shows the displacement at the same point in an uncracked plate.

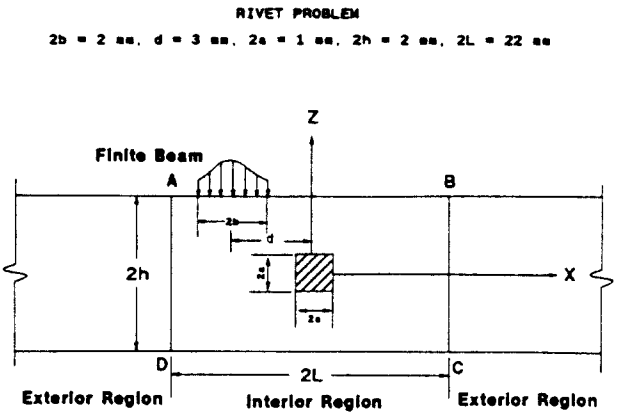

Fig. 10. Schematic diagram of a rivitted plate geometry.

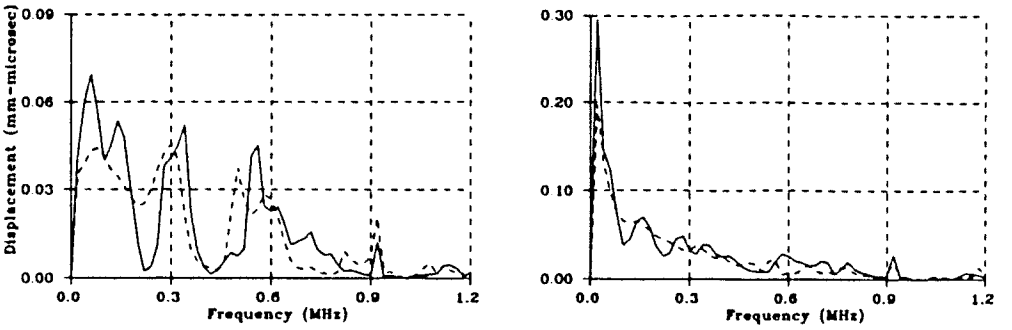

Fig. 11. Left and right columns show the horizontal and normal surface displacements at point (2.0, 1.0) for the rivetted plate geometry shown in Fig. 10. Dashed line shows the displacement at the same point for homogeneous plate.

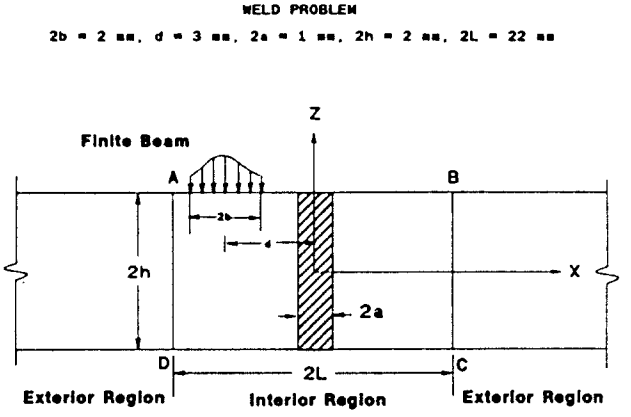

Fig. 12. Schematic diagram of a welded plate geometry.

The surface response of two aluminum plates joined by a weld (properties in Table 1), as shown in Fig. 12, is shown in Fig. 13. Here also the finite element mesh shown at the bottom of Fig. 2 are used with the appropriate change of material properties of the elements in the weld position. The magnitude of the displacement spectra can be seen to be decreased because of the stiffer welded joint. The effect of the weld is greater on the horizontal displacement than on the vertical displacement because of the vertical orientation of the weld.

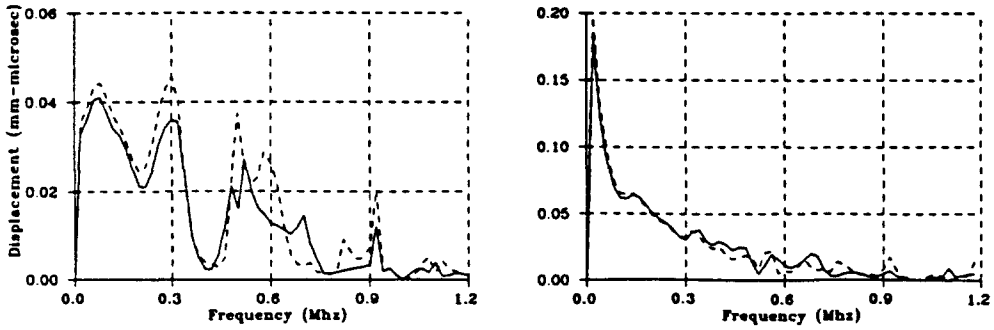

Fig. 13. Left and right columns show the horizontal and normal surface displacements at point (2.0, 1.0) for the plate geometry shown in Fig. 12. Dashed line shows the displacement at the same point in a homogeneous plate.

4. CONCLUDING REMARK

A versatile technique based on the global–local approach is presented to simulate the surface source/surface receiver ultrasonic non-destructive evaluation experiments. The method presented here can be used to calculate the response of a plate containing cracks and inclusions subjected to any type of time-dependent loading such as impact, cyclic, etc. Results presented here sometimes show significant and sometimes insignificant differences between responses of homogeneous and inhomogeneous (due to internal cracks or inclusions) plates.

Acknowledgement—This research was partially supported by the National Science Foundation under contract Number DMC-8807661.

REFERENCES

Avanessian, V., Dong, S. B. and Muki, R. (1989). Interaction of an axisymmetric body with obliquely incident seismic waves by global–local finite elements. *Earthq. Engng Struct. Dynamics* **18**, 185–197.

Barsoum, R. S. (1976). On the use of isoparametric finite elements in liner fracture mechanics. *Int. J. Numer. Meth. Engng* **10**, 25–37.

Duke, J. C., Henneke, E. G. and Stinchcomb, W. W. (1986). Ultrasonic stress wave characterization of composite materials. NASA CR-3976.

Henshell, R. D. and Shaw, K. G. (1975). Crack tip finite elements are unnecessary. *Int. J. Numer. Meth. Engng* **9**, 495–507.

Karim, M. R., Awal, M. A. and Kundu, T. (1992). Numerical analysis of guided wave scattering by cracks in a plate: SH-case. *Engng Fract. Mech., Int. J* (in press).

Karim, M. R. and Kundu, T. (1990). Scattering of acoustic beams by cracked composite. *ASCE J. Engng Mech.* **116**, 1812–1827.

Karim, M. R., Mal, A. K. and Bar-Cohen, Y. (1990). Inversion of leaky Lamb wave data by simplex algorithm. *J. Acoust. Soc. Am.* **88**(1), 482–491.

Kundu, T. (1988). Acoustic microscopy at low frequency. *ASME J. Appl. Mech.* **55**, 545–550.

Kundu, T. and Hassan, T. (1987). A numerical study of the transient behavior of an interface crack in a bimaterial plate. *Int. J. Fract.* **35**, 55–69.

Lancaster, P. (1969). *Theory of Matrices*. Academic Press, New York.

Lynn, P. P. and Ingraffea, A. R. (1978). Transition elements to be used with quarter-point crack tip elements. *Int. J. Numer. Meth. Engng* **12**, 1031–1036.

Mal, A. K. and Singh, S. J. (1990). *Deformation of Elastic Solids*. Prentice-Hall, Englewood Cliffs, NJ.

Paskaramoorthy, R., Shah, A. H. and Datta, S. K. (1989). Scattering of fluxural waves by a crack in a plate. *Engng Fract. Mech.* **33**(4), 589–598.

Romanel, C. and Kundu, T. (1990). Soil-structure interaction in a layered medium. *Int. J. Engng Sci.* **28**, 191–213.

Tang, B. and Henneke, E. G. (1989). Lamb wave monitoring of axial stiffness reduction of laminated composite plate. *Mater. Eval.* **47**, 928–934.

Xu, P. C. and Mal, A. K. (1987). Calculation of the in-plane Green's functions for a multilayered viscoelastic solid. *Bull. Seism. Soc. Am.* **77**, 1823–1837.